JOURNAL OF Applied Polymer SCIENCE

Lubrication of Poly(vinyl alcohol) Chain Orientation by Carbon Nano-Chips in Composite Tapes

Kenan Song, Yiying Zhang, Jiangsha Meng, Marilyn L. Minus
Department of Mechanical and Industrial Engineering, Northeastern University, 360 Huntington Avenue, Boston, MA 02115-5000

Correspondence to: M. L. Minus (E-mail: m.minus@neu.edu)

ABSTRACT: The extraordinary structural properties of graphene and carbon nanotube materials motivate the development of practical methods for their use in fabricating continuous, strong, and tough composite fibers. Poly(vinyl alcohol) (PVA)/carbon nano-chip fiber (CNCF) composite tapes with 0.5 wt % loading show that Young's modulus, tensile strength, and toughness are increased by 585%, 653%, and 20%, respectively as compared to the control (PVA) tapes. Nano-chips exfoliated from the CNCF during processing, lubricate polymer chain alignment, and orientation during drawing, where composite tapes could be drawn to higher draw ratios compared with the control tapes. As a result, the Herman's orientation factor (f) increased from 0.5 (control tape) to 0.8 (composite tape). Theoretical analysis shows $\sim$ 16 vol % of the composite tapes consists of fully oriented PVA chains, which contributes to its exceptional mechanical performance. © 2012 Wiley Periodicals, Inc. J. Appl. Polym. Sci. 000: 000–000, 2012

KEYWORDS: nano-composites; crystallinity; tapes; nanotubes; PVA; fibers

Received 13 March 2012; accepted 26 April 2012; published online
DOI: 10.1002/app.37963

INTRODUCTION

Similar to carbon nanotubes, interest in graphene (be it in the form of platelets/sheets, ribbons, stacked fibers, or chips) is mainly due to their excellent mechanical,[1,2] electrical,[3,4] and thermal properties.[5] In addition, graphene has also been reported as one of the strongest materials measured (i.e., modulus $\sim$ 1 TPa and tensile strength $\sim$ 130 GPa).[2] For researchers working with engineering polymers, incorporating high strength and modulus graphitic materials into the polymer matrix is very attractive for improvement in mechanical performance. Some polymers studied include, poly(methyl methacrylate),[6,7] epoxy,[8] poly(vinyl alcohol) (PVA),[9–11] nylon-6,[12,13] nylon-12,[14] polyacrylonitrile,[15] polystyrene,[16] polyelectrolyte,[17] poly(lactic acid),[18] polyurethane,[19,20] polyamide,[21] chitosan,[22,23] and polycarpolactone.[24]

There are several key aspects for polymer/graphitic composite materials design and mechanical behavior: (i) the structural control and preservation of the nano-fillers; (ii) the dispersions of isolated graphene layers or individual (exfoliated) nanotubes within the polymer matrix; and (iii) the interfacial interactions between the nano-filler and the polymer chains. Structural control of the graphitic materials is mostly influenced by synthesis processes, and this would determine their aspect ratio, morphology and dimensions, crystalline structure, purity, and properties.[25] Obtaining homogeneous dispersions of nano-fillers in the polymer matrix remains a challenge; however, it has been achieved using several methods including, chemical and physical functionalization,[26–28] as well as mechanical dispersion.[10,15] Good interfacial bonding between matrix and filler provide effective stress transfer, which at the macroscale result in strengthening or hardening of the composite materials. Mechanisms for interfacial interactions in nano-composites include weak van der Waals, micromechanical interlocking, as well as chemical bonding.[29–32]

PVA has also been extensively used as reinforcement fibers for concrete materials to retard fracture or crack initiation, due to its relatively high modulus and strength, adhesive strength, and alkali resistance. With further development of PVA nano-composites, it is expected that stronger PVA fibers could be used to replace steel fibers in concrete.[33] So far, PVA has been extensively studied in conjunction with various nano-carbons like graphene,[26–28] and single-wall carbon nanotubes (SWNT) to fabricate high-performance fibers and composite films.[10,34–37] Several of these studies have shown the ability of these nano-carbon filler to modify and influence the morphology of the PVA in the composite.[10,38,39] These nucleation, crystallization, and orientation effects are especially observed in composites with low nano-carbon loading (<1 wt %), and have a

significant impact on the overall structure and properties of the composite material.[10,15] Fundamental knowledge of how these nano-fillers influence the polymer morphology during composite processing is still lacking. Therefore, it is beneficial to study the effects of low loadings of nano-carbons in polymer composites to understand their role on polymer morphology formation.

In this work, the effect of adding carbon nano-chip fibers (CNCF) (i.e., stacked nano-fibers consisting of few-wall carbon nanotubes [FWNT] with aspect ratio $\sim$ 1) into PVA composite tapes is studied. By introducing a low concentration of CNCF (0.5 wt % loading) into the PVA matrix (i.e., without either chemical modification or addition of surfactant), a dramatic enhancement in chain orientation during tape drawing is observed for the composite as compared with the control tapes. The nano-chips act to lubricate polymer chain extension. Therefore, composite tapes exhibit well-development long-range crystalline order, and as a result, significant modulus and tensile strength improvement is also observed.

EXPERIMENTAL

Materials

As-produced, nano-chips (i.e., flattened FWNT with aspect ratio $\sim$ 1, consisting of six to eight walls) stack to form nano-fibers. CNCFs were purchased from Catalytic Materials LLC (width $\sim$ 100 nm, average length $\sim$ 1000 nm, purity $>$ 99 wt %, density $\sim$ 2.2 g·cm^{-3}, and surface area $\sim$ 120 m^2·g^{-1}). Mowiol 56–98 PVA (M_w $\sim$ 105,600 g·mol^{-1}) was obtained from Kuraray America. Dimethyl sulfoxide (DMSO) was purchased from Fisher Scientific (CAS# 67-68-5, lot# 092053). All the materials were used as-received without further modification.

Preparation of Control PVA and Composite Tapes

The PVA solution was made by dissolving 30.8 g PVA into 200 mL DMSO at $\sim$ 90°C. For the composite solution, 6.6 g of PVA was first dissolved into 100 mL DMSO, then 154 mg of CNCF was added into the polymer solution and sonicated (Fisher F530 bath sonicator, 43 kHz, 150 W) for 24 h until optically homogeneous dispersions were formed. Subsequently, 24.2 g of PVA and an additional 100 mL DMSO was added to the PVA/CNCF/DMSO dispersion. The additional PVA was dissolved at $\sim$ 90°C, and the entire solution was stirred for 24 h to obtain an optically homogenous spinning dope. The overall solid concentration of the CNCF in the dope was 0.5 wt %.

Both the control PVA and PVA/CNCF composite tapes were spun using dry-jet wet spinning. The solutions were extruded using a syringe pump (Nexus 6000, manufactured by Chemyx) through a slit die (0.125 inches by 50 μm) at a rate of 4 mL·min^{-1}. The as-spun tapes passed through a methanol coagulation bath maintained at room temperature (25°C) and were collected on take-up rollers (rate $\sim$ 10 m·min^{-1}). The tapes were further soaked in methanol for additional 2 days before being dried and drawn on rectangular hot plate (10 inches by 1 inch) for five stages from 100 to 180°C at a step-size of 20°C.

Characterizations

The fracture surfaces of the control PVA tapes and PVA/CNCF tapes drawn up to 180°C were observed using a field-emission high-resolution scanning electron microscope (SEM) (Zeiss Surpa 25, accelerating voltage 5 kV). Transmission electron microscopy (TEM) was performed on a JEOL 2010 microscope operated at 200 kV, and the samples were deposited on holey carbon coated 200 mesh copper grid (Electron Microscopy Sciences Lot#110622). Wide-angle and small-angle X-ray diffraction/scattering was performed using a S-MAX 3000 + 007 HFM WAXS/SAXS system operated at 1.2 kW with a beam focal size of 70 μm, equipped with a 200 mm multiwire two dimensional detector, manufactured by Rigaku Americas. Small-angle and wide-angle X-ray diffraction (WAXD)/scattering patterns were analyzed using Rigaku NANO-Solver^{TM} and Jade MDI software's to obtain azimuthal integration data as well as peak widths (i.e., full-width at half maximum [FWHM]). Tensile tests were conducted using dynamic mechanical analyzer (RSA-G2 series, manufactured by TA instruments) with the gauge gap of 20 mm and the extension rate of 0.1 mm·min^{-1}. The number of samples tested ranged from 5 to 10. Thermal tests were performed using a differential scanning calorimeter (DSC) (Q200, manufactured by TA Instruments). A heating rate of 10°C·min^{-1} was used under air flow from $\sim$ 40°C to 300°C. Thermogravimetric analysis (TGA) (Q50, manufactured by TA Instruments) was also conducted with a heating rate of 20°C·min^{-1} under air flow from $\sim$ 25°C to 900°C.

RESULTS AND DISCUSSION

The fracture surfaces of the control PVA tapes and PVA/CNCF tapes drawn up to 180°C were observed using SEM and shown in Figure 1(a, b). Figure 1(c) shows the SEM image for the as-received CNCF. The CNCF resemble flat wrinkled or kinked fibers, which consists of nano-chips stacked perpendicular to the CNCF axis [Figure 1(d)]. It is believed that during processing the CNCF are shortened and distorted due to the exfoliation of the nano-chips (flattened nanotubes) from the CNCF [Figure 1(e, g)]. SEM of the sonicated CNCF [Figure 1(f)] shows that they are indeed shorter as compared with the as-received powder. Based on TEM analysis [Figure 1(g)], it is observed that the sliding of nano-chips platelets from the CNCF occurs during sonication.

WAXD patterns for the PVA and PVA/CNCF tapes are shown in Figure 2(a, b). Based on these diffraction patterns, it is clear that the orientation of the PVA chains along the tape axis is much higher in the composite than for the control. Herman's orientation factor (f) was calculated using Wilchinski's approach.[39,40] The Wilchinsky equation [eq. (1)] was modified to calculate the b axis chain orientation for PVA using predominant (101) and (200) crystallographic planes[10]. Wilchinsky's relationship can be used to determine the orientation along the PVA chain axis as the planes chosen contain the b axis (i.e., the b axis is unique-*[h0l]* planes are chosen). $\langle \cos^2 \varphi_{(h0l)} \rangle$ was determined using eq. (2) which incorporated the integrated azimuthal data for the (101) and (200) crystallographic planes. Based on Wilchinsky's equation, $\langle \cos^2 \theta \rangle_{b-\text{axis}}$ was determined for both the control and composite tapes. Herman's orientation function [eq. (3)] was then used to obtain Herman's orientation factor (f) for each of the tapes. For both the control and composite tapes, f was found to be 0.5 and 0.8, respectively. During spinning, PVA/CNCF tapes could be drawn to a ratio of 10, while PVA fibers could only be

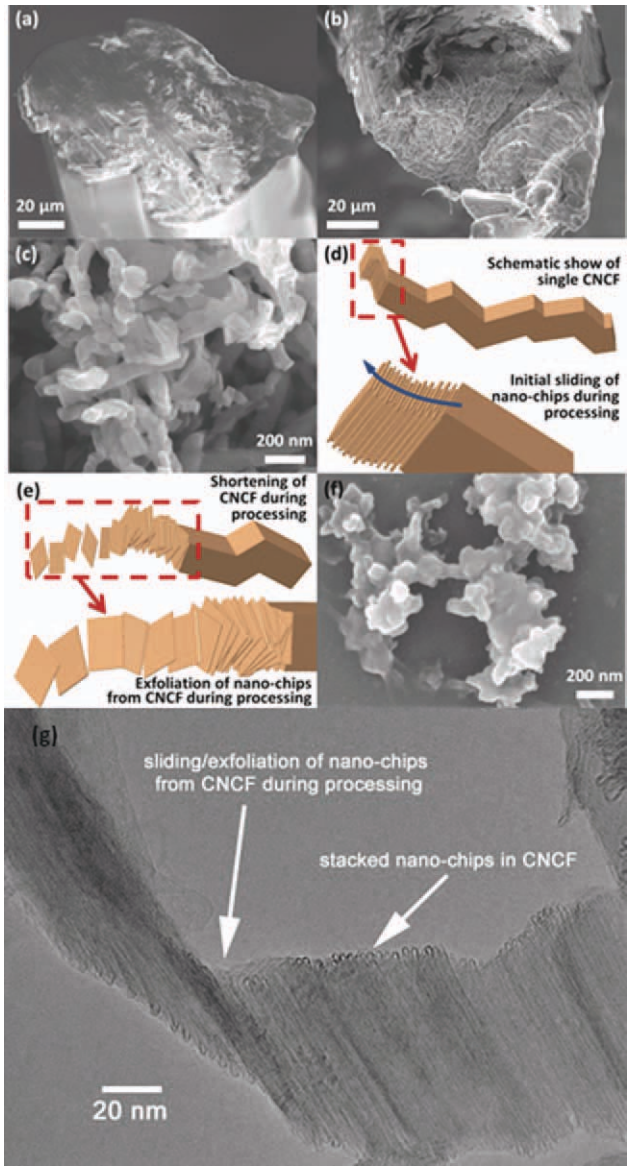

Figure 1. SEM images of fracture surfaces for the (a) PVA and (b) PVA/CNCF tapes. (c) SEM of the as-received CNCF powder. Schematics of CNCF showing (d) the stacking of the nano-chips along the CNCF axis, and (e) the sliding and exfoliation of the nano-chips from the CNCF during processing. (f) SEM of the sonicated PVA/CNCF solution. (g) Transmission electron microscope (TEM) image of sonicated CNCF showing the sliding of the nano-chip platelets from the fiber during processing. [Color figure can be viewed in the online issue, which is available at wileyonlinelibrary.com.]

drawn to 6 (Table I). It is believed that the exfoliated nano-chips act as a lubricating material within the tape to facilitate polymer chain slippage, extension, and orientation.

$$\langle \cos^2 \theta \rangle_{b-axis} = \frac{(1 - 2\sin^2 \rho_2)\langle \cos^2 \varphi_1 \rangle - (1 - 2\sin^2 \rho_1)\langle \cos^2 \varphi_2 \rangle}{\sin^2 \rho_1 - \sin^2 \rho_2} \quad (1)$$

Where, the subscripts 1 and 2 corresponds the each of the crystal planes used, and ρ is the angle between the plane normal and a or c axis.[10]

$$\left\langle \cos^2 \varphi_{(h0l)} \right\rangle = \frac{\int_0^{\pi/2} I(\varphi) \cos^2 \varphi \ \sin \varphi \ d\varphi}{\int_0^{\pi/2} I(\varphi) \sin \varphi \ d\varphi} \quad (2)$$

where, $I(\varphi)$ is the azimuthal intensity for a specific diffraction peak integrated over the azimuthal angle φ.

$$f = \frac{3\langle \cos^2 \theta \rangle_{b-\text{axis}} - 1}{2} \quad (3)$$

Based on small-angle X-ray scattering (SAXS) analysis it was also found that for both tapes a peak is observed along the meridian [Figures 2(c, d)]. This peak indicates periodic stacks of crystalline lamellae orientated along the tape axis. The long-order spacing was measured to be 12.5 nm for the control tape and 17.4 nm for the composite tape [Figure 2(e, f)]. In conjunction with higher orientation shown from the WAXD data, the PVA/CNCF tapes clearly display larger periodic stacking of the crystalline lamellae based on SAXS experiments.

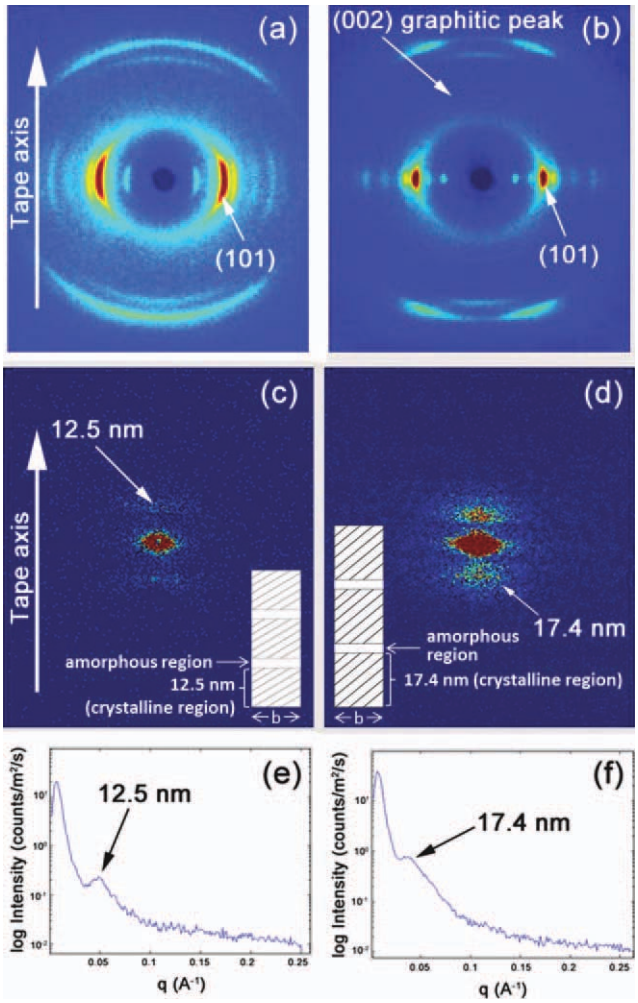

Figure 2. WAXD images of (a) PVA, (b) PVA/CNCF tapes. SAXS images of (c) PVA and (d) PVA/CNCF tapes. Intensity versus q, SAXS curves for (e) PVA and (f) PVA/CNCF tapes. [Color figure can be viewed in the online issue, which is available at wileyonlinelibrary.com.]

Table I. Thermal and Mechanical Properties of PVA and PVA/CNCF Tapes

Sample	PVA	PVA/0.5 wt % CNCF
ΔH_m, (J·g^{-1})	80.6	80.4
X_c[a] (%)	58.2	58.0
T_m[b] (°C)	221.8	220.9
T_g[c] (°C)	74.9	76.0
T_d[d] (°C)	293.8	302.9
Draw ratio	6	10
E[e] (GPa)	7.3 ± 1.1	50.0 ± 4.4
σ[f] (GPa)	0.17 ± 0.03	1.28 ± 0.11
ε_{max}[g] (%)	18.3 ± 2.8	5.3 ± 0.7
Toughness, (J·g^{-1})	16.1 ± 5.0	28.9 ± 7.5

[a]Crystallinity degree (X_c) was calculated using ΔH_m (ΔH_c for PVA is 138.6 J·g^{-1}),[41] [b]Melting temperature, [c]Glass transition temperature, [d]Degradation temperature, [e]Young's modulus, [f]Tensile stress, [g] Elongation strain.

Overall crystallinity in the materials was measured using DSC and calculated from the enthalpy of melting (ΔH_m) (see Table I). The overall crystallinity and melting temperatures are comparable in both composite and control tapes [Table I, Figure 3(a)]. TGA was also performed on the tapes. It was observed that the degradation temperature for the PVA/CNCF composite fiber increased by ~ 9°C after the addition of the CNCF [Table I, Figure 3(b)]. This increase may be due to the exfoliation of the nano-chips throughout the polymer matrix, thereby increasing the thermal stability.[5,42]

The mechanical properties for both PVA and PVA/CNCF tapes were measured using a tensile test, and these properties are listed in Table I. The stress-strain curves are shown in Figure 3(c). Based on these measurements it is found that there is a 585% increase in the modulus and 653% increase in the tensile strength. These results are significantly higher than typical percent increases reported for Young's modulus and tensile strength in polymer-based nano-composite fiber.[43] As mentioned earlier, the CNCF loading is only 0.5 wt %, and based on WAXS data [Figure 2(b)] the overall orientation of the nano-chips along the fiber axis is relatively low (i.e., [002] peak of the graphitic plane). Therefore, the improvement in modulus and tensile strength is mostly attributed to changes in the polymer morphology as facilitated by the presence of the CNCF.

The modulus contribution ($V_f E_f$) of the nano-chip fibers to the composite properties was calculated using the rule-of-mixture analysis for uniaxial composites [eq. (4)].[44]

$$E_c = V_f E_f + V_{m1} E_{m1} \quad (4)$$

where, E_c, E_{m1}, and E_f are the Young's moduli of the composite, matrix, and the fiber, respectively, and V_{m1} and V_f are the volume fractions of the matrix and fiber.

The bulk modulus (E_{m1}) for the PVA is taken as the experimentally measured modulus of the control tape, while the filler modulus (E_f) is taken from various experimentally and theoretically attained moduli for graphitic based materials (i.e., SWNTs, multiwall carbon nanotubes (MWNT), single-layer graphene (SLG), few-layer graphene (FLG), and SWNT bundles), and these values are listed in Table II. It is immediately obvious that the modulus contribution of the nano-filler is very low at the volume fraction used, even when the nano-carbon is assumed to be fully oriented along the fiber axis. In addition, if the misorientation of the CNCF and nano-chips is considered as shown by X-ray diffraction (Figure 2), the modulus

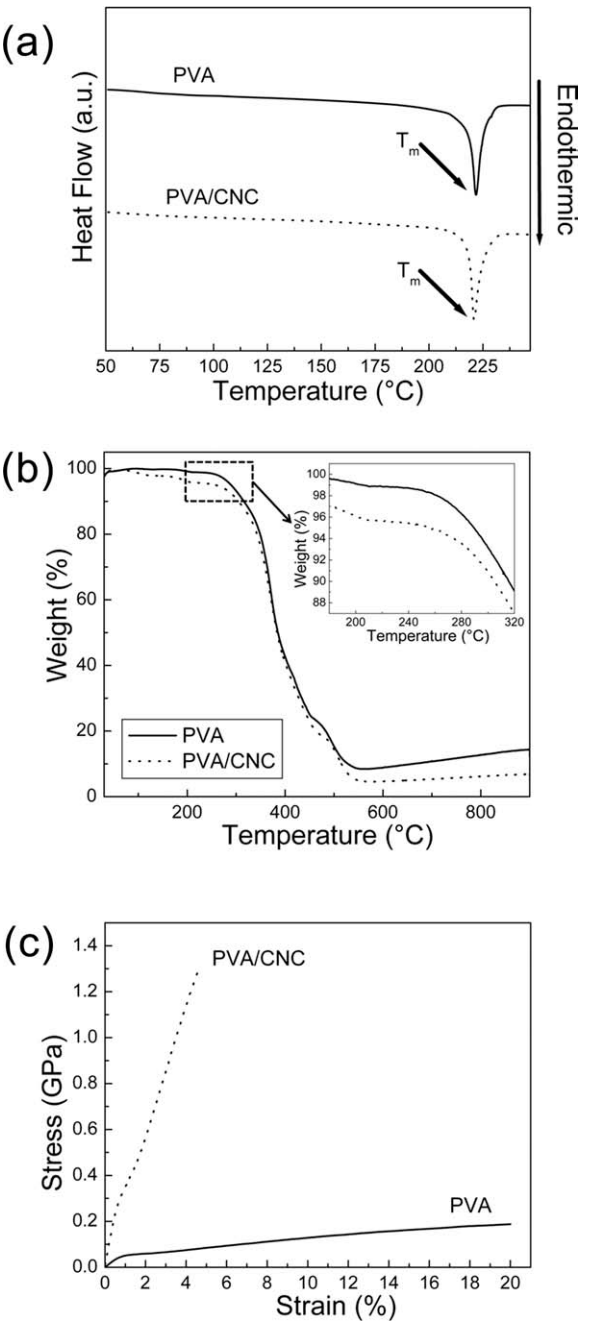

Figure 3. (a) DSC of control PVA and PVA/CNCF tapes drawn to 180°C showing similar melting transition. (b) TGA showing behavior degradation of PVA and PVA/CNCF tapes, and (c) stress-strain curves of the drawn control and composite fibers.

Table II. Rule-of-Mixture Evaluation for PVA and PVA/CNCF Tapes[a]

	Nano-Carbons	E_f[b] (GPa)	V_fE_f (GPa)	$V_{m1}E_{m1}$[c] (GPa)	$V_{m2}E_{m2}$[d] (GPa)	V_{m2} (%)
Fully oriented	SWNT	1002[45]	3.0	6.2	38.6	15.1
	MWNT	1800[46]	5.4	6.3	38.3	14.2
	SLG	1000[2]	3.0	6.3	38.6	15.1
	FLG	700[47]	2.1	6.3	39.5	15.5
		500[48]	1.5	6.3	40.1	15.7
		8.31[49]	0.02	6.1	41.5	16.3
Misaligned	SWNT rope[e]	23[50]	0.07	6.1	41.4	16.3

[a] $V_f = 0.3$ vol % is the volume fraction of CNCF fillers, [b] E_f is the axial modulus of nanofillers, [c] $E_{m1} = 7.3$ Gpa., [d] $E_{m2} = 255$GPa[51], [e]SWNT bundles ($\sim$ 4.5 nm diameter) were misoriented with the average angle $\langle\theta\rangle \sim 39^\circ$ (Herman's orientation factor $f \sim 0.388$).

contribution becomes negligible (see Table II). For this reason, to analyze the origin for the large improvement in tensile properties for the PVA versus PVA/CNCF tapes, the rule-of-mixture equation is modified to include a component associated with oriented PVA chains ($V_{m2}E_{m2}$) [eq. (5)]. The theoretical modulus used for fully oriented PVA chains in the axial direction is $\sim$ 255 GPa.[51]

$$E_c = V_f E_f + V_m 1 E_m 1 + V_m 2 E_m 2 \quad (5)$$

where, the E_{m2}, and V_{m2} are the Young's modulus and the volume fraction of the oriented PVA.

As mentioned earlier, microstructural analysis of the PVA and PVA/CNCF tapes by SAXS shows the existence of long-order crystalline regions oriented along the tape axis in both materials. The PVA/CNCF tapes show larger crystalline lamellae stacking along the tape axis which is $\sim$ 5 nm thicker than the control tapes. The width of the crystal lamellar stack (b) is also determined from the FWHM for the peak using the Scherrer equation [eq. (6)].[52,53]

$$b = \frac{\lambda}{\Delta(2\theta)_{0.5}} \quad (6)$$

Where, λ is the wave-length of the X-ray (0.154 nm), $\Delta(2\theta)_{0.5}$ is the width of the diffraction spot at half peak intensity measured. The FWHM [$\Delta(2\theta)_{0.5}$] was measured directly from the SAXS peaks for the control and composite tapes (Figure 2) data using the curve fitting capability of the NANO-Solver™ SAXS software.

This width (b) was determined to be $\sim$ 15.7 nm for both control and composite tapes. Based on this data, it is determined that the microstructure of the tapes consists of parallel crystalline stacks of the same width with differing thickness, and this is illustrated in the insets of Figure 2(c, d). Qualitatively it can also be observed from the SAXS patterns [Figure 2(c)] that the long-order peak for the control sample shows more diffused scattering as compared with the composite, this may indicate a larger variation of the crystalline stack thickness or the existence of more interdispersed amorphous material as compared with the composite. As the overall orientation for the control tape is much lower than the composite tape (i.e., $f = 0.5$ [control]; $f =$ 0.8 [composite]), these regions of oriented crystalline stacks are assumed to play a large role in the overall increase of the mechanical properties of the tapes.

Orientation of the PVA chains as well as the formation of such large crystalline domains is facilitated by the sliding processes and exfoliation of the nano-chips from the CNCF. The nano-chips lubricate PVA chain slippage and facilitate alignment in the fibers, leading to large well-formed crystalline domains. The presence of these aligned regions greatly contributes to the improvement of the mechanical properties of the composite tape. Based on eq. (5), it is found that to achieve the experimental composite modulus of 50 GPa the volume percentage of oriented crystalline PVA regions in the fiber is $\sim$ 16 vol %.

CONCLUSIONS

This work brings to light the ability of these unique nano-fillers act as a lubricant to facilitate polymer chain extension. As such, stiffness and strength increase in the composite material are due to the inherent properties of the polymer that occur because of morphological changes. The fractional addition of the nano-filler is also able to improve the thermal stability of the composite. This provides a novel route for producing high-performance composite materials from flexible polymers by only using a small amount of these carbon nano-filler, thereby having a negligible effect on the cost of the composite.

ACKNOWLEDGMENTS

Financial support of this work was provided by Air Force Office of Scientific Research (AFOSR) (FA9550-11-1-0153) and start-up funding from Northeastern University.

REFERENCES

1. Shokrieh, M. M.; Rafiee, R. *Mater. Des.* **2010,** *31*, 790.
2. Lee, C.; Wei, X.; Kysar, J. W.; Hone, J. *Sci.* **2008,** *321*, 385.
3. Castro Neto, A. H.; Guinea, F.; Peres, N. M. R.; Novoselov, K. S.; Geim, A. K. *Rev. Mod. Phys.* **2009,** *81*, 109.
4. Stoller, M. D.; Park, S.; Zhu, Y.; An, J.; Ruoff, R. S. *Nano Lett.* **2008,** *8*, 3498.

5. Balandin, A. A.; Ghosh, S.; Bao, W. Z.; Calizo, I.; Teweldebrhan, D.; Miao, F.; Lau, C. N. *Nano Lett.* **2008,** *8*, 902.
6. Ramanathan, T.; Abdala, A. A.; StankovichS; Dikin, D. A.; Herrera Alonso, M.; Piner, R. D.; Adamson, D. H.; Schniepp, H. C.; Chen, X.; Ruoff, R. S.; Nguyen, S. T.; Aksay, I. A.; Prud'Homme, R. K.; Brinson, L. C. *Nat. Nano.* **2008,** *3*, 327.
7. Goncalves, G.; Marques, P.; Barros-Timmons, A.; Bdkin, I.; Singh, M. K.; Emami, N.; Gracio, J. J. *Mater. Chem.* **2010,** *20*, 9927.
8. Rafiee, M. A.; Rafiee, J.; Wang, Z.; Song, H. H.; Yu, Z. Z.; Koratkar, N. *ACS Nano* **2009,** *3*, 3884.
9. Zhao, X.; Zhang, Q. H.; Chen, D. J.; Lu, P. *Macromolecules 43*, 2357 **2010.**
10. Minus, M. L.; Chae, H. G.; Kumar, S. *Macromol. Chem. Phys.* **2009,** *210*, 1799.
11. Young, K.; Blighe, F. M.; Vilatela, J. J.; Windle, A. H.; Kinloch, I. A.; Deng, L.; Young, R. J.; Coleman, J. N. *ACS Nano.* **2010,** *4*, 6989.
12. Li, C. Y.; Li, L.; Cai, W.; Kodjie, S. L.; Tenneti, K. K. *Adv. Mater.* **2005,** *17*, 1198.
13. Xu, Z.; Gao, C. *Macromolecules* **2010,** *43*, 6716.
14. Rafiq, R.; Cai, D. Y.; Jin, J.; Song, M. *Carbon* **2010,** *48*, 4309.
15. Chae, H. G.; Minus, M. L.; Kumar, S. *Polymer* **2006,** *47*, 3494.
16. Fang, M.; Wang, K. G.; Lu, H. B.; Yang, Y. L.; Nutt, S. J. *Mater. Chem.* **2009,** *19*, 7098.
17. Kulkarni, D. D.; Choi, I.; Singamaneni, S. S.; Tsukruk, V. V. *ACS Nano.* **2010,** *4*, 4667.
18. Cao, Y. W.; Feng, J. C.; Wu, P. Y. *Carbon* **2010,** *48*, 3834.
19. Khan, U.; May, P.; O'Neill, A.; Coleman, J. N. *Carbon* **2010,** *48*, 4035.
20. Kim, H.; Miura, Y.; Macosko, C. W. *Chem. Mater.* **2010,** *22*, 3441.
21. Chen, D.; Zhu, H.; Liu, T. X. *ACS Appl. Mater. Interfaces* **2010,** *2*, 3702.
22. Han, D. L.; Yan, L. F.; Chen, W. F.; Li, W. *Carbohydr. Polym.* **2011,** *83*, 653.
23. Wang, X. L.; Bai, H.; Yao, Z. Y.; Liu, A. R.; Shi, G. Q. *J. Mater. Chem.* **2010,** *20*, 9032.
24. Cai, D. Y.; Song, M. *Nanotechnology* **2009,** *20*, 6.
25. Terrones, M.; Botello-Méndez, A. R.; Campos-Delgado, J.; López-Urías, F.; Vega-Cantú, Y. I.; Rodríguez-Macías, F. J.; Elías, A. L.; Muñoz-Sandoval, E.; Cano-Márquez, A. G.; Charlier, J. C.; Terrones, H. *Nano. Today* **2010,** *5*, 351.
26. Das, B.; Prasad, K. E.; Ramamurty, U.; Rao, C. N. *R. Nanotechnology* **2009,** *20*, 5.
27. Yang, X. M.; Li, L. A.; Shang, S. M.; Tao, X. M. *Polymer* **2010,** *51*, 3431.
28. Xu, Y. X.; Hong, W. J.; Bai, H.; Li, C.; Shi, G. Q. *Carbon* **2009,** *47*, 3538.
29. Satti, A.; Larpent, P.; Gun'ko, Y. *Carbon* **2010,** *48*, 3376.
30. Bai, H.; Li, C.; Shi, G. Q. *Adv. Mater.* **2011,** *23*, 1089.
31. Potts, J. R.; Dreyer, D. R.; Bielawski, C. W.; Ruoff, R. S. *Polymer* **2011,** *52*, 5.
32. Sengupta, R.; Bhattacharya, M.; Bandyopadhyay, S.; Bhowmick, A. K. *Prog. Polym. Sci.* **2010,** *36*, 638.
33. Xu, X.; Uddin, A. J.; Aoki, K.; Gotoh, Y.; Saito, T.; Yumura, M. *Carbon* **2010,** *48*, 1977.
34. Vigolo, B.; Penicaud, A.; Coulon, C.; Sauder, C.; Pailler, R.; Journet, C.; Bernier, P.; Poulin, P. *AIP Conf. Proc.* **2001,** *591*, 562.
35. Zhang, X. F.; Liu, T.; Sreekumar, T. V.; Kumar, S.; Moore, V. C.; Hauge, R. H.; Smalley, R. E. *Nano lett.* **2003,** *3*, 1285.
36. Dalton, A. B.; Collins, S.; Munoz, E.; Razal, J. M.; Ebron, V. H.; Ferraris, J. P.; Coleman, J. N.; Kim, B. G.; Baughman, R. H. *Nature* **2003,** *423*, 703.
37. Wang, Z.; Ciselli P.; Peijs, T. *Nanotechnology* **2007,** *18*, 455709.
38. Minus, M. L.; Chae, H. G.; Kumar, S. *Polymer* **2006,** *47*, 3705.
39. Minus, M. L.; Chae, H. G.; Kumar, S. *Macromol. Rapid Commun.* **2010,** *31*, 310.
40. Wilchinsky, Z. W. *J. App. Phys.* **1960,** *31*, 1969.
41. Peppas, N. A.; Hansen, P. J. *J. Appl. Polym. Sci.* **1982,** *27*, 4787.
42. Guo, H. N.; Minus, M. L.; Jagannathan, S.; Kumar, S. *ACS Appl. Mater. Interfaces* **2010,** *2*, 1331.
43. Kuilla, T.; Bhadra, S.; Yao, D. H.; Kim, N. H.; Bose, S.; Lee, J. H. *Prog. Polym. Sci.* **2010,** *35*, 1350.
44. Derek H.; Clyne, T. W., Introduction to Composite Materials; Cambridge University Press: Cambridge, **1996.**
45. Yu, M. F.; Files, B. S.; Arepalli, S.; Ruoff, R. S. *Phys. Rev. Lett.* **2000,** *84*, 5552.
46. Treacy, M. M. J.; Ebbesen, T. W.; Gibson, J. M. *Nature* **1996,** *381*, 678.
47. Rasuli, R.; Zad, A. I.; Ahadian, M. M. *Nanotechnology* **2010,** *21*, 185503.
48. Frank, I. W.; Tanenbaum, D. M.; Zande, A. M. v. d.; McEuen, P. L. J. *Vac. Sci. Technol. B* **2007,** *25*, 2558.
49. Poot, M.; van der Zant, H. S. *J. App. Phys. Lett.* **2008,** *92*, 063111.
50. Liu, T.; Kumar, S. *Nano lett.* **2003,** *3*, 647.
51. Sakurada, I.; Ito, T.; Nakamae, K., *J. Polym. Sci. Part C: Polym. Symp.* **1967,** *15*, 75.
52. Allen, G.; Bevington, J. C.; Booth, C.; Price, C. In Comprehensive Polymer Science: The Synthesis, Characterization, Reactions & Applications of Polymers; Hall, I. H., Ed.; Pergamon Press, cop.: New York, **1990.**
53. Hall, I. H.; Mahmoud, E. A.; Carr, P. D.; Geng, Y. D. *Colloid Polym. Sci.* **1987,** *265*, 383.